SUPPLEMENTAL MATERIAL

Lie algebraic solution of time dependent Lindblad equation

Here, we describe in detail the Lie algebraic method used to solve the time dependent Lindblad equation [S1–S7]. Our starting point is to treat the b mode semiclassically by replacing $\hat{b}$-operators with a c-number, $\hat{b} \to b$. This simplification allows us to solve the rest of the equation for the a-mode exactly using the Lie-algebraic approach since the remaining quantum operators form a closed Lie algebra. Using this approach we can keep track of any possible time dependencies exactly. Note that for time independent system parameters the semiclassical solution is in fact the exact solution to this system. For the driving protocol used in this work, time independence of the system parameters can be achieved through a rotating wave transformation. Here, however, we solve the system for any arbitrary choice of time dependent system parameters. For the a-mode from equation (2) in the main text we have

$$\dot{\rho} = -i\left[\omega_a \hat{a}^\dagger \hat{a} + g b^*(t)\hat{a} + g^* b(t)\hat{a}^\dagger, \rho\right] + \frac{\gamma_a}{2}\mathcal{D}[\hat{a}]\rho \equiv \mathcal{L}\rho, \tag{S.1}$$

whereas for the b-mode in the semiclassical limit we find:

$$i\dot{b} = i\kappa_b\, b + g\langle\hat{a}\rangle + iK|b|^2 b + E_1(t)^*. \tag{S.2}$$

where $K = -\chi_b - iU$ and $\kappa_b = -\gamma_b/2 - i\omega_b$. Eqs. (S.1) and (S.2) form a coupled system. Together they provide a self-consistent solution to equation (2) in the main text in the absence of quantum fluctuations in the b-mode. Our quantum mechanical problem is therefore reduced to that of a simple harmonic oscillator with time dependent coherent drive and dissipation. In order to solve the system of Eqs (S.1) and (S.2) for any choice of the time dependent parameters, we can use the Lie-algebraic properties of the operators. The main idea behind this approach is that the time-evolution operator, being a time-ordered exponent, is an element of a Lie group, as long as the operators in the Liouvillian (S.1) form a closed Lie algebra. When this algebraic structure holds, one can make a solution ansatz of the following form:

$$\rho(t) = \prod_j e^{c_j(t)O_j}\rho(0), \tag{S.3}$$

where $c_j(t)$ are time dependent functions that depend on the system parameters, and O_j are the systems superoperators. Defining the commutator for two superoperators O_1 and O_2 as

$$[O_1, O_2]\rho = O_1(O_2\rho) - O_2(O_1\rho), \tag{S.4}$$

and identifying the superoperators in Eq. (S.1) (i.e. the set of O_j's in (S.3)) as

$$\begin{aligned} &J\rho = a\,\rho a^\dagger, \quad B_L\rho = a^\dagger a\rho, \quad B_R\rho = \rho a^\dagger a, \\ &A_L\rho = a\rho, \quad A_L^\dagger\rho = a^\dagger\rho, \quad A_R^\dagger\rho = \rho a, \quad A_R\rho = \rho a^\dagger, \end{aligned} \tag{S.5}$$

we find that these superoperators generate the following Lie algebra:

$$\begin{aligned} &[A_L, A_L^\dagger] = 1, && [A_R, A_R^\dagger] = 1 \\ &[B_L, A_L] = -A_L, && [B_R, A_R] = -A_R, \\ &[B_L, A_L^\dagger] = A_L^\dagger, && [B_R, A_R^\dagger] = A_R^\dagger \\ &[B_L, J] = -J, && [B_R, J] = -J, \\ &[J, A_L^\dagger] = A_R, && [J, A_R^\dagger] = A_L, \end{aligned} \tag{S.6}$$

with all other commutators being zero. In terms of these superoperators, Liouvillian (S.1) can be written as

$$\mathcal{L} = \kappa_a B_L + \kappa_a^* B_R + \gamma_a J + igb^*\left(A_R^\dagger - A_L\right) + ig^* b\left(A_R - A_L^\dagger\right), \tag{S.7}$$

where we introduce the same parameters $\kappa_a = -i\omega_a - \gamma_a/2$ as in the main text. Since the Liouvillian is generated by elements forming the closed Lie algebra, the solution to (S.1) is given by a product of *ordinary* (opposed to the time-ordered in the general case) time dependent exponentials of the form in eq. (S.3) Obviously, the choice for this

type of representation is not unique (e.g it could depend on the ordering of individual factors), however if for $\rho(0)$ we pick up a coherent initial state

$$\rho(0) = |\alpha_0\rangle\langle\alpha_0|\,, \tag{S.8}$$

then a natural choice for the ordering of the products would be the of the form

$$\rho(t) = e^{f(t)}\, e^{h(t)J}\, e^{\beta(t)B_L}\, e^{\beta^*(t)B_R} e^{\alpha(t)A_L^\dagger} e^{-\alpha^*(t)A_L}\, e^{\alpha^*(t)A_R^\dagger} e^{-\alpha(t)A_R}\, \rho(0). \tag{S.9}$$

Here, the relationships between the different time dependent functions $c_j(t)$ can be derived from the hermiticity of the density matrix $\rho(t)$. Note the presence of the prefactor $\exp[f(t)]$. It appears because the Lie algebra in Eq. (S.6) is spanned not only by the superoperators (S.5), but it also contains the identity operator, as can be seen from the commutation relations. The Ansatz in Eq. (S.9) is one of the most natural ones because the action of the group elements on the initial state (S.8) is very simple. Differentiating $\rho(t)$ in Eq. (S.9) and using various adjoint actions (in order to commute all exponentials to the right), such as

$$\begin{aligned}
&e^{gJ}\, B_L\, e^{-gJ} = B_L + gJ, && e^{gJ}\, B_R\, e^{-gJ} = B_R + gJ, && e^{gJ}\, A_R^\dagger\, e^{-gJ} = A_R^\dagger + gA_L,\\
&e^{gJ}\, A_L^\dagger\, e^{-gJ} = A_L^\dagger + gA_R, && e^{gA_R}\, B_R\, e^{-gA_R} = B_R + gA_R, && e^{gA_R}\, A_R^\dagger\, e^{-gA_R} = A_R^\dagger + g,\\
&e^{gA_R^\dagger}\, J\, e^{-gA_R^\dagger} = J - gA_L, && e^{gA_R^\dagger}\, B_R\, e^{-gA_R^\dagger} = B_R - gA_R^\dagger, && e^{gA_R^\dagger}\, A_R\, e^{-gA_R^\dagger} = A_R - g,\\
&e^{gA_L}\, B_L\, e^{-gA_L} = B_L + gA_L, && e^{gA_L}\, A_L^\dagger\, e^{-gA_L} = A_L^\dagger + g, && e^{gA_L^\dagger}\, J\, e^{-gA_L^\dagger} = J - gA_R,\\
&e^{gA_L^\dagger}\, B_L\, e^{-gA_L^\dagger} = B_L - gA_L^\dagger, && e^{gA_L^\dagger}\, A_L\, e^{-gA_L^\dagger} = A_L - g, && e^{gB_R}\, J\, e^{-gB_R} = e^{-g}\, J,\\
&e^{gB_R}\, A_R\, e^{-gB_R} = e^{-g}\, A_R, && e^{gB_R}\, A_R^\dagger\, e^{-gB_R} = e^{g}\, A_R^\dagger, && e^{gB_L}\, J\, e^{-gB_L} = e^{-g}\, J,\\
&e^{gB_L}\, A_L\, e^{-gB_L} = e^{-g}\, A_L, && e^{gB_L}\, A_L^\dagger\, e^{-gB_L} = e^{g}\, A_L^\dagger,
\end{aligned} \tag{S.10}$$

we get

$$\begin{aligned}
\dot\rho = \Big\{ &\dot\beta^* B_R + e^{\beta^*}\dot\alpha^* A_R^\dagger + \left(he^{\beta} - e^{-\beta^*}\right)\dot\alpha A_R + \dot\beta B_L + e^{\beta}\dot\alpha A_L^\dagger\\
&+ \left(he^{\beta^*} - e^{-\beta}\right)\dot\alpha^* A_L + \left[\dot h + h\left(\dot\beta + \dot\beta^*\right)\right] J + \dot f + \partial_t|\alpha|^2 \Big\}\,\rho(t).
\end{aligned} \tag{S.11}$$

Matching the expression in the curly brackets with Liouvillian (S.7), we obtain a system of differential equations for $f(t)$, $h(t)$, $\alpha(t)$, and $\beta(t)$:

$$\begin{aligned}
&\dot\beta = \kappa_a, && \dot h - \gamma_a h - \gamma_a = 0,\\
&\dot\alpha = -ig^* b e^{-\beta}, && \dot f + \partial_t|\alpha|^2 = 0,
\end{aligned} \tag{S.12}$$

with zero initial conditions. Note that the above equations are coupled with the semiclassical equation for the b-mode Eq. (S.2). This particular system of differential equations, Eqs. (S.12), can be solved in terms of quadratures as follows:

$$\begin{aligned}
&\beta(t) = \int_0^t d\tau\, \kappa_a(\tau), && \alpha(t) = -i\int_0^t d\tau\, e^{-\beta(\tau)} g^*(\tau) b(\tau),\\
&h(t) = e^{-(\beta(t)+\beta^*(t))} - 1 = e^{\int_0^t d\tau\, \gamma_a(\tau)} - 1, && f(t) = -|\alpha(t)|^2,
\end{aligned} \tag{S.13}$$

where $b(t)$ is a solution to Eq. (S.2). Indeed, taking into account the definitions of $A_{L,R}\rho$ and $A_{L,R}^\dagger\rho$, along with the expression for the displacement operator in terms of a and $a^\dagger$,

$$|\alpha_0\rangle = D(\alpha_0)\,|0\rangle = e^{-|\alpha_0|^2/2} e^{\alpha_0 a^\dagger} e^{-\alpha_0^* a}\,|0\rangle\,, \tag{S.14}$$

where $|\alpha_0\rangle$ is a coherent state, the action of the last four exponents in Eq. (S.9) can be written as

$$e^{|\alpha(t)|^2} D(\alpha(t))\,|\alpha_0\rangle\langle\alpha_0|\, D(-\alpha(t)) = e^{|\alpha(t)|^2}\,|\alpha_0 + \alpha(t)\rangle\langle\alpha_0 + \alpha(t)|\,. \tag{S.15}$$

Here we took into account that $|\alpha_0\rangle\langle\alpha_0| = D(\alpha_0)\,|0\rangle\langle 0|\, D(-\alpha_0)$ and used the following property of the displacement operators: $D(\alpha)D(\alpha_0) = \exp\{\alpha\alpha_0^* - \alpha^*\alpha_0\}D(\alpha_0+\alpha)$. Note that the exponential prefactor cancels with the factor of

$e^{f(t)}$ in Eq. (S.9). It is now straightforward to calculate the action of the remaining exponentials in the first line of Eq. (S.9) on the state $|\alpha_0+\alpha(t)\rangle\langle\alpha_0+\alpha(t)|$. Using the fact that

$$e^{\beta^* a^\dagger a}\,|v\rangle = e^{-|v|^2/2}\sum_{n=0}^{+\infty}\frac{\left(v\,e^{\beta^*}\right)^n}{\sqrt{n!}}\,|n\rangle = \exp\left\{\frac{|v\,e^{\beta^*}|^2-|v|^2}{2}\right\}\left|v\,e^{\beta^*}\right\rangle, \tag{S.16}$$

where $|v\rangle$ is a coherent state, we get

$$e^{\beta^* B_L}\,e^{\beta B_R}\,|\alpha_0+\alpha\rangle\langle\alpha_0+\alpha| = e^{\left(e^{2\mathrm{Re}\{\beta\}}-1\right)|\alpha_0+\alpha|^2}\left|(\alpha_0+\alpha)e^{\beta^*}\right\rangle\left\langle(\alpha_0+\alpha)e^{\beta^*}\right|. \tag{S.17}$$

Finally, the action of $\exp(hJ)$ is trivially found using the formal power series expansion of the exponent

$$e^{hJ}\,|v\rangle\langle v| = \sum_{n=0}^{+\infty}\frac{h^n}{n!}\,a^n\,|v\rangle\langle v|\,\left(a^\dagger\right)^n = e^{h|v|^2}\,|v\rangle\langle v|\,. \tag{S.18}$$

In our case this yields

$$e^{hJ}\left|(\alpha_0+\alpha)e^{\beta^*}\right\rangle\left\langle(\alpha_0+\alpha)e^{\beta^*}\right| = \exp\left\{h\,e^{2\mathrm{Re}(\beta)}\,|\alpha_0+\alpha|^2\right\}\left|(\alpha_0+\alpha)e^{\beta^*}\right\rangle\left\langle(\alpha_0+\alpha)e^{\beta^*}\right|. \tag{S.19}$$

Then, taking into account that $h\,\exp\left[2\mathrm{Re}(\beta)\right] = 1-\exp\left[2\mathrm{Re}(\beta)\right]$, as follows from Eq. (S.13), we combine Eqs. (S.15), (S.17), and (S.19), and observe that all exponential prefactors cancel out. Thus, the density matrix from Eq. (S.9) reduces to

$$\rho(t) = \left|\left(\alpha_0+\alpha(t)\right)e^{\beta(t)}\right\rangle\left\langle\left(\alpha_0+\alpha(t)\right)e^{\beta(t)}\right|. \tag{S.20}$$

This exact solution allows us to compute the expectation value of $\hat{a}(t)$ as

$$\alpha(t) = \langle a(t)\rangle = \mathrm{Tr}\left[\hat{a}\rho(t)\right] \tag{S.21}$$

thus effectively reducing our problem to solving the following set of coupled differential equations,

$$\begin{aligned} i\dot{\alpha} =& g^* e^{-\beta} b, \\ i\dot{b} =& i\kappa_b\, b + g e^{\beta}\,(\alpha_0+\alpha) + iK|b|^2 b + E_1(t)^*. \end{aligned} \tag{S.22}$$

Our problem can further be reduced to an autonomous system of equations by assuming that g, κ_a, κ_b, and U are time-independent, and the driving amplitude being an oscillatory function $E_1(t) = \mathcal{E}_1 e^{i\omega_1 t}$. In this case, using an appropriate chance of variables,

$$\begin{aligned} y(t) &= e^{\beta(t)+i\omega_1 t}\big(\alpha_0+\alpha(t)\big), \\ z(t) &= e^{i\omega_1 t} b(t), \end{aligned} \tag{S.23}$$

one can reduce Eq. (S.22) to

$$\begin{aligned} \dot{y} =& \tilde{\kappa}_a y - i g^* z, \\ \dot{z} =& -igy + \tilde{\kappa}_b z + K|z|^2 z - i\mathcal{E}_1^* \end{aligned} \tag{S.24}$$

which is used to find the results reported in equation (3) in the main text.

Weak interaction limit

The system we consider here is, technically speaking, a zero dimensional system, and as such there is no obvious concept of taking a thermodynamic limit. However, Casteels et al. [S8] made a inspirational argument based on the works of Carmicheal [S9]: they compared the Fourier transforms of the Liouvillian (S.1) and a system of N copies of dissipative coherently driven Bose-Hubbard chains, where N is the number of cavities. This resembles a thermodynamic limit. The suggested equivalence can readily be derived by substituting Fourier transformed bosonic operators into the Hamiltonian for the 1D Bose Hubbard chain. Note that the homogeneous drive corresponds only

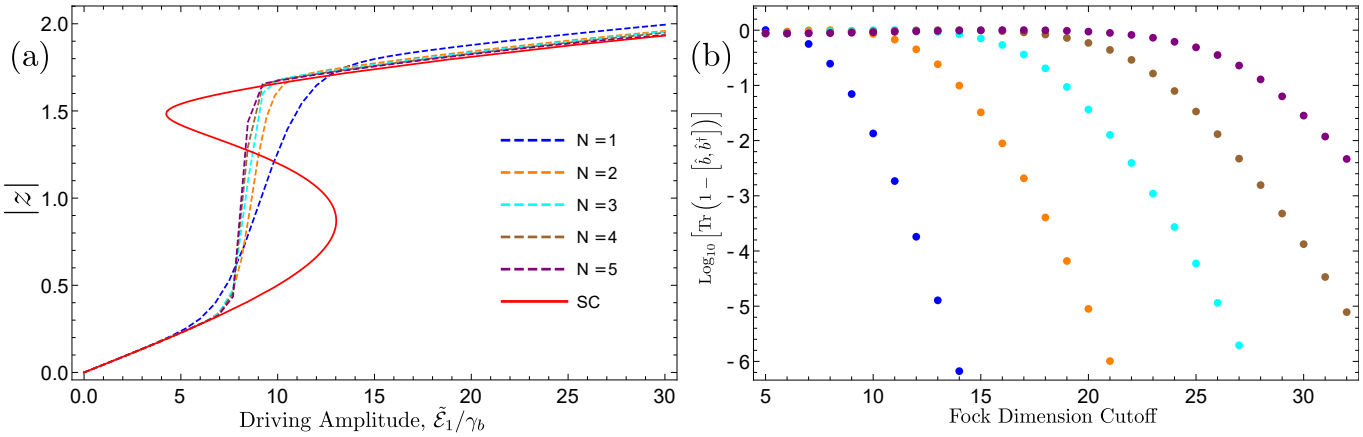

FIG. S1. (a) Comparison of semi classical steady state solution as a function of $\tilde{\mathcal{E}}_1/\gamma_b$ (Red curve) and the numerically computed, exact solutions of the steady state using a truncated Fock space representation of the bosonic a and b modes (dashed curves). The parameters are $g = 5$, $\arg \mathcal{E}_1 = 0$, $\gamma_a = \chi_b = 1$, $\Delta_a = U = 10$ and $\Delta_b = -20$ (in units of γ_b). Cutoff dimensionality for both modes is based on the results from Fig (b) and are 17, 17, 24, 28, 30 for the modes $N = 1 \ldots 5$ respectively. (b) Convergence of steady-state expectation value Tr $\left(\hat{b}^\dagger \hat{b} \rho_{ss}\right)$ measured by evaluating Tr $\left(1 - [\hat{b}^\dagger, \hat{b}]\right)$ for different values of N. The closer this value is to zero, the better the convergence is. Fock space dimensionality cutoff is the same for both the a- and b-modes. The parameters are are the same as in Fig (a). The convergence is measured at the point $\tilde{\mathcal{E}}_1/\gamma_b = 30$ which requires the largest dimensionality of the Hilbert space to converge, since the steady state particle number increases as a function of $\tilde{\mathcal{E}}_1$.

to the $k = 0$ mode in the expansion. The only difference between the arguments made in [S8] and this work is that we also added a two-mode dissipation channel. This results in rescaling the parameters $\mathcal{E}_1$, U and the dissipation rate χ. The scaling of χ turns out to be the same as that of U. Omitting the details of the trivial calculation we conclude that we need to rescale the system parameters as follows

$$\mathcal{E}_1 = \tilde{\mathcal{E}}_1 \sqrt{N}, \qquad U = \frac{\tilde{U}}{N}, \qquad \chi = \frac{\tilde{\chi}}{N}. \tag{S.25}$$

Using this notion of thermodynamic limit we can perform numerical computations to probe the full quantum phase diagram of our system. Fig. S1(a) shows that the quantum mechanical description of the system converges to the semiclassical prediction as we increase N, the steady state expectation value of the particle number operator. Note that in the quantum regime there is no bi-stability because of the single-valuedness of the wavefunction. Instead, we observe a sharp transition. The increase in the slope of the transition is expected to grow proportionally to N, as confirmed by this plot. The datapoints in Fig. S1(a) have been computed using a cutoff representation of the a- and b-mode operators in the Hilbert space. This numerical approximation scheme relies on the assumption that our system dynamics are for the largest part contained in the small particle number subspace. Thus we write the Liouvillian in the (infinite dimensional) number basis for the creation and annihilation operators and cut off the rank of the resulting matrices for the $\hat{a}$ and $\hat{b}$ operators to some finite value [S11]. This value is determined by varying the rank of the resulting matrices and monitoring the convergence of the quantum state, as was done in Fig. S1(b). In Fig S1(b), we were looking at the steady state expectation value of the operator $1-[\hat{b}, \hat{b}^\dagger]$ which should be zero for a high convergence. The datapoints in the figure are taken at $\tilde{\mathcal{E}}_1/\gamma_b = 3.0$, which requires the largest cutoff values to converge in the data set corresponding to this figure. We would like to note that the full quantum mechanical Liouvillian scales as $\text{Rank}(\hat{a})^2 \times \text{Rank}(\hat{b})^2$. By increasing the value of N, the steady state expectation values of $\text{Tr}(\hat{a}^\dagger \hat{a} \rho(t))$ and $\text{Tr}(\hat{b}^\dagger \hat{b} \rho(t))$ steadily increase and spread out, requiring larger cutoffs in the Hilbert space. Direct eigenvalue solver algorithms using LU decomposition (e.g. in the ARPACK library) scale rather expensively in their RAM consumption. For steady state calculations we can use a trick to increase the computational efficiency. We introduce a new matrix $O = L^\dagger L$, where L is the vectorized Liouvillian. The zero eigenvector $\vec{\rho}$ of O is the steady-state solution of L. This can be shown by considering the relationship of the kernel of the new matrix $O\rho = L^\dagger(L\vec{\rho}) = 0 \iff L\vec{\rho} \in \text{Ker}(L^\dagger)$. Since isomorphisms leave kernels invariant, this implies that $L^\dagger \vec{\rho} \in \text{Ker}(L) \implies L^\dagger \vec{\rho} = 0$. Thus, the zero eigenvector of O is the same as that of L and $L^\dagger$. This hermitization of the density matrix L allows us to compute eigenvalues and vectors for the Liouvillian L through the hermitian matrix O using Cholesky decomposition in combination with a shift-invert method [S10]. This algorithm requires significantly less RAM compared to sparse LU-decomposition, at the cost of a less sparse matrix that needs to be diagonalized. Using this approach, the largest matrix size that

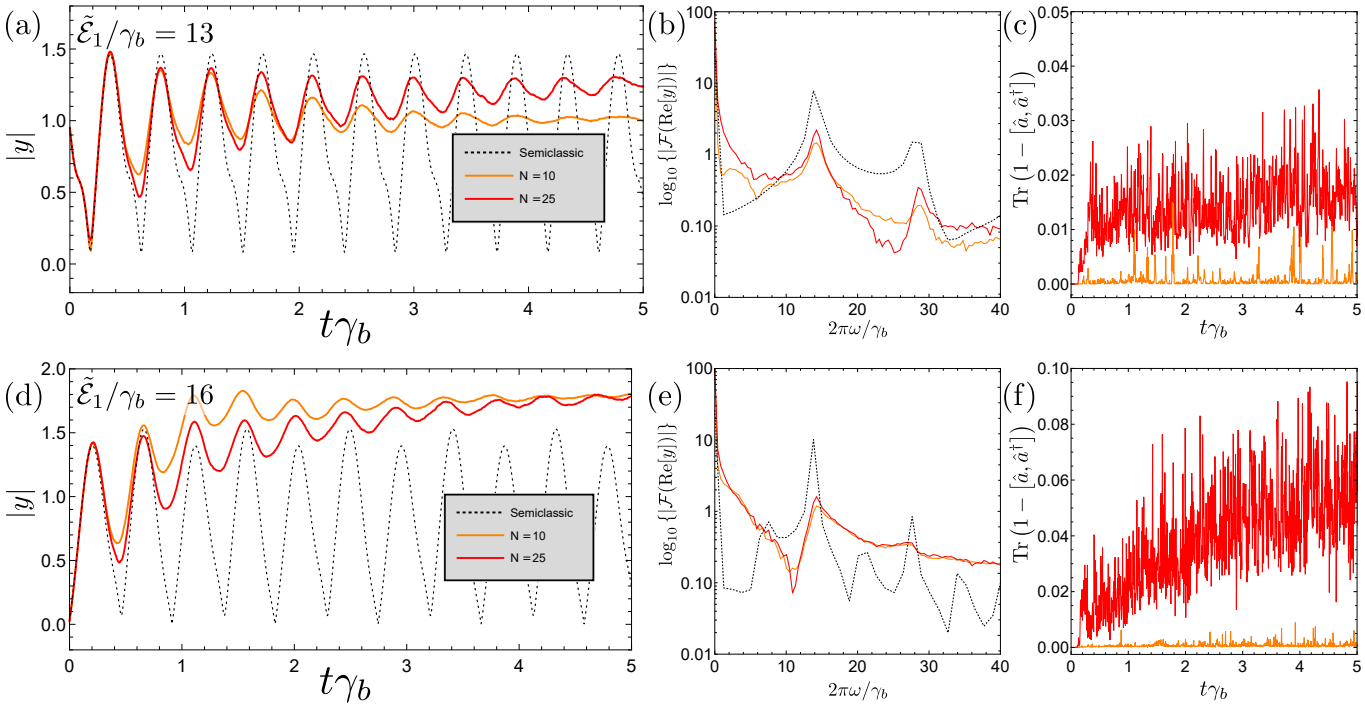

FIG. S2. Monte Carlo trajectories of particle number expectation values $y = \mathrm{Tr}[\hat{a}^\dagger\hat{a}\rho(t)]$. Figs. (a), (b) and (c) show the averaged quantum trajectories at a driving amplitude of $\tilde{\mathcal{E}}_1/\gamma_b = 13$, the associated Fourier spectrum and error. The orange and red lines show the behavior for $N = 10$ and $N = 25$ respectively with Fock-dimension cutoffs of 100 and 250. The semiclassical prediction is also included (dashed black lines). The initial state of the quantum trajectories is a coherent state, with an expectation value predicted by the semiclassical solutions. The quantum trajectories have been computed for a total time of $t_{\mathrm{total}}\gamma_b = 15$, with $dt\gamma_b = 0.005$ and averaged over 3000 individual trajectories. Figs. (d), (e) and (f) show the same as the figures in the row above, but now at a driving amplitude of $\tilde{\mathcal{E}}_1/\gamma_b = 16$. Note that for this driving amplitude, the system decays faster to the steady state. This is expected from the larger dissipative gap at this parameter choice. The period doubled mode is visible in the semiclassical regime in the Fourier spectrum in figure (e). All parameters in the figure are the same as in the figures of main text.

we could diagonalize had Hilbert space dimensionalities equal to 32 for both the a- and b modes. This corresponds to a matrix size of order $\approx 10^6$, with a total RAM requirement of ≈ 1 TB and ≈ 6 hours of computation time per datapoint using the MATLAB software.

For the excited modes a trick like the one mentioned above will not work and one has to resort to using sparse LU-decompositions. Using this method we can compute the eigenvalues presented in the main text up to a cutoff of the Hilbert space dimension equal to 31. We note, however, that this is not enough to ensure high convergence for e.g. the period doubling modes for $N = 3$ and 4. Nevertheless, we can qualitatively extrapolate the behavior of this system for higher values of N as we did in the main text. Larger computational power, or more efficient schemes should be used to probe the period doubling behavior in more detail.

Monte Carlo trajectories

In order to overcome the limitations of direct diagonalization we studied the quantum trajectories of the system using the QuTiP package for python [S11]. This procedure is less sensitive to scaling of matrix sizes, and allows for larger system sizes up to $N = 25$ at a cutoff in Hilbert space dimensions (in the number basis) by 250. Results are shown in Fig. S2. We clearly see that the trajectories decay to a steady state expectation value. This is coming from the fact that the dissipative gap is still finite. Increasing the parameter N slows down the decay. From the Fourier spectrum we determine the periodicity of oscillations which closely match our semiclassical predictions. The period doubling mode remains elusive from these figures. This is a result of the choice of the initial state plugged into the computations. For the trajectories shown in Fig. S2, we have chosen a coherent initial state on a point of the limit cycle predicted by the semiclassical analysis. This state has a negligible overlap with the period doubled mode, which

can be deduced using the results of exact diagonalization methods for small values of N. Therefore, the quantum trajectories are exceedingly unlikely to exhibit period doubling in their Fourier spectrum at the level of precision of the computations in this work. In essence, we have simply started the system out in the basin of attraction of the regular time crystal, rather than the period doubled time crystal phase. We note that this does not imply that any phase of matter is dependent on the choice of the initial state. Rather, using trajectories and initial states inherently pushes one to a specific phase, simply due to basins of attraction for each possible phase in the system. Despite this flaw, the method of quantum trajectories can be used to probe phases of a system due to it's low memory requirements in computations. As long as one is aware of this method's shortcomings, trajectories can still reveal interesting results.

[S1] V. Gritsev and A. Polkovnikov, SciPost Phys. **2**, 021 (2017).
[S2] M. Ringel and V. Gritsev, Phys. Rev. A **88**, 062105 (2013).
[S3] L. R. Bakker, V. I. Yashin, D. V. Kurlov, A. K. Fedorov, and V. Gritsev, Phys. Rev. A **102**, 052220 (2020).
[S4] S. Charzyński and M. Kuś, J. Phys. A: Math. Theor. **46**, 265208 (2013).
[S5] J. Wei and E. Norman, J. Math. Phys. **4**, 575 (1963).
[S6] J. Wei and E. Norman, Proc. Am. Math. Soc. **15**, 327 (1964).
[S7] M. O. Scully and M. S. Zubairy, *Quantum Optics* (Cambridge University Press, 1997).
[S8] W. Casteels, R. Fazio, and C. Ciuti, Phys. Rev. A **95**, 012128 (2017).
[S9] H. J. Carmichael, Phys. Rev. X **5**, 031028 (2015).
[S10] F. Pietracaprina, N. Macé, D. J. Luitz, and F. Alet, SciPost Phys. **5**, 45 (2018).
[S11] J. Johansson, P. Nation, and F. Nori, Comput. Phys. Commun. **184**, 1234 (2013)